Understanding the Component-Driven Influence on the Electrochemical Properties in Single-Ion Polymer Electrolytes for Sodium-Based Batteries

Clemens Wunder, Leo Graeber, Dominic Bresser, Maider Zarrabeitia,* and Stefano Passerini*

ABSTRACT: Research on polymer electrolytes has attracted growing attention in recent years as they offer increased mechanical and thermal stability compared to liquid electrolytes, making them excellent candidates for metal batteries. Their properties can be fine-tuned depending on the need, allowing, for example, the creation of single-ion polymer electrolytes (SIPEs) that could suppress dendrite formation and charge gradient buildups. This work describes the optimization of a Na-SIPE consisting of sodium salt monomer (SSM), pentaerythritol tetraacrylate (PETA4), pentaerythritol tetrakis(3-mercaptopropionate) (PETMP), and poly(vinylidene fluoride-*co*-hexafluoropropylene) (PVDF-HFP), by varying the composition ratio of the SIPE components. In addition, the influence on ionic conductivity and overall performance in Na-based cells of three different anionic centers of SSM is reported. The best electrochemical performance is achieved with a content of 17 mol% SSM, 18 mol% PVDF-HFP, 40 mol% PETMP, and 25 mol% PET4A due to the highest ionic conductivity. The optimal SSM is found to be (4-styrenesulfonyl)(dicyano)methanide (NaSDCM), enabling the NaSDCM-based SIPE to achieve a conductivity of 2.9×10^{-4} S cm^{-1} at 90 °C and 4.2×10^{-5} S cm^{-1} at 20 °C, thermal stability up to 300 °C, and electrochemical stability window up to 5 V vs Na^+/Na. This SIPE with 50 wt% molecular transporter enables the realization of Na||SIPE||Prussian White (PW) cells, delivering a specific capacity of 102 mAh g^{-1} after 200 cycles at 0.1C and 40 °C.

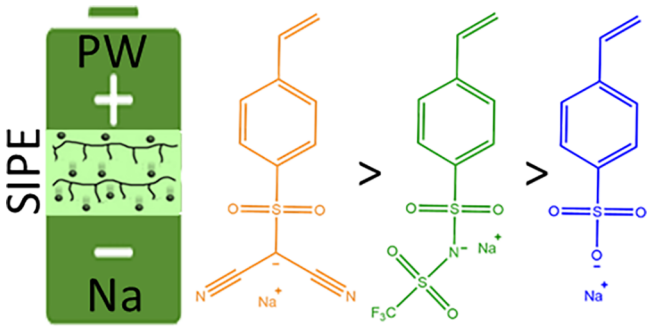

KEYWORDS: *single-ion polymer electrolyte, quasi-solid-state electrolyte, anionic center, sodium salt monomer, sodium batteries, polymer optimization*

INTRODUCTION

Lithium-ion batteries (LIBs) have been a cornerstone for economic growth in the past years,[1] and they are estimated to grow to reach a global production of 1200 GWh by 2025.[2] However, this growing production comes with tremendous challenges due to the scarcity of lithium and other metals (*e.g.*, cobalt). The International Energy Agency study projects that cobalt demand will rise from 190 kt in 2023 to 454 kt in 2024. Similarly, the demand for lithium is expected to increase significantly, from 170 to 1,330 kt, taking into account both primary and secondary supply as well as reuse.[3] Thus, alternative energy storage chemistries employing abundant and sustainable resources have caught the interest of both academia and industry.[4−8]

One potential alternative is sodium-ion batteries (SIBs), which can be produced from sustainable and low-cost components.[9,10] Sodium is very abundant in the Earth's crust (2.4×10^4 ppm) and in the ocean (1.8×10^4 ppm) compared to lithium (20 and 180 ppm, respectively);[1] thus, various companies such as Contemporary Amperex Technology Co., Ltd. (CATL), Build Your Dreams (BYD), and Faradion have begun to commercialize SIBs for large-scale grid applications and light electric vehicles.[11−15] The anode of choice in SIBs is hard carbon. However, the use of insertion-type anode materials comes with charge-storage limitations, which result in a limited energy density. This limitation is even more concerning for SIBs compared to LIBs because Na ions are bigger, thus requiring more space for insertion while producing

more volume expansion.[16] Sodium−metal batteries (SMBs) can avoid this issue by utilizing Na metal in combination with a high-voltage cathode, resulting in an even higher specific energy density compared to SIBs. Even safer and more sustainable is the adoption of the metal-less anode configuration, consisting of the use of a plain current collector as the negative electrode and a sodiated positive electrode material for the cell assembly. In such a cell, named zero-excess sodium−metal batteries (ZESMBs), the Na is directly plated on the aluminum current collector (or any other form of current collector).[17] Both SMBs and ZESMBs are still rather challenging, posing high requirements on the electrolyte with regard to the suppression of dendrite formation and continuous side reactions. However, solid-state electrolytes, especially organic polymer electrolytes, which contain just enough plasticizers to form good interphase and reach high ionic conductivities with no risk of leakage, are considered promising candidates to solve these challenges since they hinder dendrite formation and increase the thermal stability up to 250 °C. For example, the 4-styrene sulfonyl (trifluoromethanesulfonyl) imide (NaSTFSI)-PET-MP/4A-PVDF-HFP SIPE with 50 wt.% of carbonate-based molecular transporter developed by our group exhibits a thermal stability up to 280 °C,[18] while the liquid electrolytes start decomposing around 100 °C.[19,20]

Organic polymer electrolytes are of special interest for SMBs and ZESMBs due to their high flexibility, self-standing properties, good conductivity, modularity, and excellent mechanical and thermal properties.[21−23] In SIPEs, the cation is the only mobile species, while the anion is covalently tethered to the polymer backbone, thus rendering it immobile in contrast to the dual-ion polymer electrolytes where both cation and anion are mobile. The anion immobilization, chemically bonded to the polymer backbone, results in high transference numbers close to unity, allowing for more efficient Na^+ transport. Moreover, since only the cation is mobile in the SIPEs, they can suppress the buildup of concentration gradients generated by the anions, which move faster than the cations, thereby counteracting the movement of the cations upon current flow. Preventing anion concentration gradients circumvents the internal resistance that normally builds up when cycling at high rates, thus enabling high charge/discharge current rates while avoiding dendrite growth.[24,25]

SIPEs are easily tunable by changing their components, as well as their respective ratios. Thus, they are easily adjusted to match various requirements. For example, the SIPE's thickness and mechanical stability can be increased to support batteries that undergo high mechanical stress, while chemical components can be modified to support, *e.g.*, higher or lower temperature operative range, higher or lower voltage window, etc.[26−32] In fact, the electrochemical properties of SIPEs depend on various factors, such as (*i*) the chemistry, flexibility, and interconnection of the backbone, (*ii*) the chemistry, size, and flexibility of the spacer arm that connects the anionic center to the backbone and (*iii*) the chemistry, strength, and accessibility of the anionic center, as well as (*iv*) the addition of additives, such as supporting polymers or plasticizers.

Previously, we have developed a NaSTFSI, PETMP, and PET4A blended with PVDF-HFP based SIPE, NaSTFSI-PET-MP/4A-PVDF-HFP, for quasi-solid-state SMBs.[18] A molecular transporter, such as a mixture containing 50 wt.% carbonate, was mixed into the SIPE, resulting in a quasi-solid-state polymer electrolyte. This electrolyte exhibits properties similar to those of solid polymer electrolyte (SPE), with the added benefit of a liquid phase integrated into the polymer matrix. This SIPE, consisting of NaSTFSI, PETMP, PET4A, and PVDF-HFP in the 9:46:25:20 molar ratio, added with 50 wt.% of carbonate-based molecular transporter, exhibited an ionic conductivity of 1.4×10^{-5} and 1.3×10^{-4} S cm^{-1} at 20 and 90 °C, respectively, high thermal stability (280 °C) and wide electrochemical stability window (up to 4.5 V vs Na^+/Na). The NaSTFSI-PET-MP/4A-PVDF-HFP SIPE implemented as electrolyte in Na||PW cells enabled delivering 147 mAh g^{-1} at 15 mA g^{-1} at 40 °C with a Coulombic efficiency of more than 99%. As a following step and to further improve the electrochemical properties of the SIPE, the effect of the concentration variations of PET4A, the supporting polymer PVDF-HFP, and NaSTFSI SSM, is herein investigated. Additionally, the impact of the charge delocalization of the anionic center is assessed by designing SSMs with different anionic centers. In fact, the anionic center influences the final properties of the SIPE. Ideally, a large anionic group delocalizes the negative charge, reducing the binding strength with the cation and allowing it to move more freely. Various anionic groups have been reported, which could be roughly categorized as carboxylate ($-CO_2-$), sulfonate ($-SO_3-$), and sulfonylimide ($-SO_2N-SO_2-$).[33,34] The interaction of the anionic group with the cation can be displayed through their dissociation energy (ΔE_d), which has been determined using DFT calculations for the lithium system using a modified styrene molecule as the salt monomer.[34] The highest dissociation energy was obtained for the $-CO_2-$ group of 4-vinylbenzoate (LiSC, 699 kJ mol^{-1}), followed by the $-SO_3-$ group of 4-styrenesulfonate (LiSS, 639 kJ mol^{-1}), the $-SO_2N-SO_2-$ group of (4-styrenesulfonyl)-(trifluoromethanesulfonyl)imide (LiSTFSI, 625 kJ mol^{-1}), and the dicyano methanide ($-C-(CN)_2$) group of (4-styrenesulfonyl)(dicyano)methide (LiSDM, 511 kJ mol^{-1}). The lowest binding energy was predicted for the $-C-(CN)_2$ group, which is even lower than the calculated binding energy of the commonly used TFSI- group, suggesting that utilizing this anionic group might support higher conductivity than the other SSMs.[34] Therefore, this work investigates the influence of different anionic centers, *i.e.*, NaSTFSI (one of the most investigated anionic groups for SIPE), sodium 4-vinylbenzenesulfonate (NaVBS, commonly used as starting anionic group for other polymers), and NaSDCM (the one showing the lowest reported binding energy, which could offer the highest ionic conductivity) in the PET-MP/4A-PVDF-HFP-based SIPE.[34] The thermal and electrochemical properties of the different SIPEs are herein assessed. Overall, the best-performing SIPE consists of NaSDCM SSM, PETPM, and PET4A blended with PVDF-HFP in a molar ratio of 4:10:7:4.4 (NaSDCM:PETMP:PET4A:PVDF-HFP), offering improved ionic conductivity, good thermal stability, a wide electrochemical stability window, and stable cycling in quasi-solid-state Na||SIPE||PW cells.

EXPERIMENTAL MATERIALS AND METHODS

Synthesis of NaSTFSI, NaSDMC, and NaVBS Sodium Salt Monomers.

NaSTFSI was synthesized using the two-step synthesis route previously reported.[18,35] NaSDCM was synthesized following the synthetic route reported by Martinez-Ibanez and co-workers (Figures S1 and S2).[34] NaVBS was bought from Sigma-Aldrich and used without further purification.

Membrane Fabrication. All SIPE membranes were prepared by the solvent casting method using a solvent mixture of dimethyl

Table 1. Composition of the dry NaSTFSI-SIPE membranes used for the evaluation of the influence of the PET4A content on the SIPE membranes.

	molar ratio [mol]				composition [mol%]	investigated factor
SIPE label	NaSTFSI	PETMP	PET4A	PVDF-HFP	NaSTFSI:PETMP:PET4A:PVDF-HFP	mol% of PET4A to PETMP
T1	2	10	4	4.4	10:49:19:22	40%
T2	2	10	5.5	4.4	9:46:25:20	55%
T3	2	10	7	4.4	9:42:30:19	70%
T4	2	10	8.5	4.4	8:40:34:18	85%
T5	2	10	10	4.4	8:38:37:17	100%

sulfoxide (DMSO, VWR chemicals, >99%) and dimethylformamide (DMF, VWR chemicals 99.8%). The two networking monomers, PETMP (Merck, 97%) and PET4A (Merck, 99%), were dissolved together with PVDF-HFP (pellets, Merck) in 7 mL DMF. Meanwhile, either NaSTFSI, NaVBS, or NaSDCM was dissolved in 1 mL DMSO. The two solutions were stirred separately for 3 h, then mixed for another 2 h, and finally cast into a Teflon disk (62 mm ⌀). After solvent evaporation at 80 °C for 28 h, self-standing SIPE membranes of around 120 μm ± 20 μm were obtained. The exact amount of the different components was varied to find the best composition as described in the Results and Discussion section. The molecular ratio that was used to investigate the influence of the anionic center using different SSMs was 17 mol% SSM, 40 mol% PETMP, 25 mol% PET4A, and 18 mol% PVDF-HFP. The obtained SIPE membranes were cut into 16 mm ⌀ discs and dried at 70 °C in vacuum for 3 h. The SIPE membranes were transferred into a glovebox (O_2 < 0.1 ppm and H_2O < 0.1 ppm) and, prior to use, swollen in 2 mL of ethylene carbonate (EC, Ube, 99%), dimethyl carbonate (DMC, Ube, 99.9%) and fluoroethylene carbonate (FEC, Ube, 99%) mixed in the 49:49:2 volume ratio at 60 °C for 48 h. The amount of solvent uptake is indicated in the Result and Discussion section reporting the PVDF-HFP content's optimization. Meanwhile, in the other investigations, the solvent uptake was around 50 wt.% ± 5 wt.% for the various SSMs and their content. The SIPE based on NaSTFSI will be labeled as NaSTFSI-SIPE, while the ones with NaVBS and NaSDCM SSMs will be referred to as NaVBS-SIPE and NaSDCM-SIPE, respectively.

Physicochemical and Thermal Characterization. The structure of the SSMs was confirmed by liquid ^{1}H, ^{13}C, and ^{19}F nuclear magnetic resonance (NMR) spectroscopy using the Bruker Avance spectrometer (400, 1H at 400 MHz) and DMSO-d6 as the solvent. The thermal properties of the SIPE membranes were evaluated using thermogravimetric analysis (TGA) performed under a He atmosphere on a Netzsch TG 209 F1 with a heating rate of 5 K min^{-1}. Before the measurement, the membrane samples (about 5 mg) were sealed in aluminum crucibles and then heated from 30 to 600 °C. Differential scanning calorimetry (DSC, Discovery series, TA Instruments) was performed on all SIPE membranes (~10 mg in sealed aluminum pans) starting from 30 °C, cooling down to −20 °C, heating up to 200 °C, and cooling back to −20 °C. The heating rate was 5 K min^{-1}, and the protection gas was N_2 (gas flow: 10 mL min^{-1}). Both TGA and DCS experiments were carried out at least two times to confirm reproducibility.

Solid Electrolyte Interphase Characterization. The formed solid electrolyte interphase (SEI) was investigated by means of X-ray photoelectron spectroscopy (XPS, SPECS) in a fixed transmission mode, using Al Kα source ($h\nu$ = 1487 eV) a Phoibos 150 XPS spectrometer (SPECS), and a Dealy Line Detector (Surface Concept). The high resolution spectra was collected at 200 W and 12 kV. Spectra were calibrated by using C−C/C−H peaks in C 1s as a reference binding energy (285 eV).[36]

Electrochemical Characterization. The electrochemical properties of the SIPE electrolytes were studied in four different coin cell configurations. The conductivity of the different SIPEs was analyzed in symmetric cells with an aluminum current collector on both sides. The conductivity was measured using electrochemical impedance spectroscopy (EIS) between 10 and 90 °C (Binder climatic chamber KB23), employing the Solartron SI 1260/1287 impedance analyzer (frequency range: 10 Hz to 1 MHz; voltage amplitude: 10 mV). Each measurement was performed after the cell rested for 3 h at the chosen temperature. The obtained impedance spectra were analyzed using the RelaxIS 3 software with an RP fit. The ionic conductivity was calculated using the formula $\sigma = d/RA$, where R is the obtained resistance from the fitting of the Nyquist plot, d is the thickness of the membrane (measured *ex-situ* using a Mitutoyo Absolute digital thickness gauge 547−401), and A is the area of the SIPE membranes.

Stripping/plating tests were performed in a symmetric Na‖SIPE‖Na configuration, applying 5 cycles at various specific current density for 1 h before reversing, starting from 10 to 50 μA cm^{-2} and cycled for another 25 cycles at 50 μA cm^{-2}. EIS was measured in a Biologic SAS VMP-3 after the first and last cycle at each current density in the frequency range of 1 kHz to 1 MHz and amplitude 10 mV at 40 °C.

The electrochemical stability windows of SIPEs were evaluated by pressing each sample between an aluminum current collector and a Na disc (12 mm ⌀) and performing linear sweep voltammetry (LSV) scans using a Biologic SAS VMP-3e. After assembling, the LSV cells were rested for 6 h and later tested at a scan rate of 30 μV s^{-1}, either up to 7 V (anodic scan) or down to −2 V (cathodic scan) vs Na^+/Na.

Finally, Na-metal cells were assembled, sandwiching the SIPEs between a PW ($Na_2Fe[Fe(CN)_6$, Altris) cathode and Na (12 mm ⌀) anode. The cells were subjected to galvanostatic tests applying a current of 0.02C (1C = 150 mAh g^{-1}) for the initial cycle, followed by 5 cycles at 0.05C and ongoing cycles at 0.1C using a Maccor 4000 battery tester. The PW electrodes consisted of 80% PW, 10% carbon 45, 5% sodium carboxymethyl cellulose (Na-CMC), and 5% styrene−butadiene rubber (SBR) with a mass loading of 1.3 mg cm^{-2} ± 0.4 mg cm^{-2}. The PW cathode was dried at 140 °C and 10^{-7} bar for 24 h and stored in a glovebox (O_2 < 0.1 ppm, and H_2O < 0.1 ppm) until assembling Na cells in coin cell (S4R CR2032) configuration. All the cells (except for ionic conductivity calculation) were run at 40 °C ± 2 °C (Binder climatic chamber KB23). The Na‖SIPE‖PW electrochemical properties were ensured by running at least three reproducible coin cells.

RESULTS AND DISCUSSION

Influence of the PVDF-HFP and NaSTFSI SSM Concentration on the NaSTFSI-Based SIPEs. The main building blocks of the NaSTFSI-SIPE are PET4A and PETMP, which bind together *via* chemical bonding of the vinyl group of PET4A and the thiol group of PETMP. The fractions of bound and unbound groups of both components are critical parameters, as an excess of one of the groups would lead to a mismatch of both components and a homopolymerization of one of the components. PET4A or PETMP-based homopolymer regions, called subclusters, are not ionically conducting since the SSM and the backbone monomers might not be in the desired ratio. Thus, the resulting structure can be considered electrochemically inactive or poorly active. Following this, these subcluster formations decrease the electrochemical performance of the SIPE. In our previous work,[18] it was confirmed that NaSTFSI-PET-MP/4A-SIPE could properly operate as a quasi-solid-state electrolyte for SMBs. To further explore compositional property enhancements, the impact of each component on the membrane

Table 2. Molar ratios of dry NaSTFSI-SIPE membranes used for the assessment of the influence of PVDF-HFP on the SIPE.

	molar ratio [mol]				composition [mol%]	investigated factor
SIPE label	NaSTFSI	PETMP	PET4A	PVDF-HFP	NaSTFSI:PETMP:PET4A:PVDF-HFP	molar% of PVDF-HFP
P1	2	10	7	0	11:53:36:0	0%
P2	2	10	7	2.2	10:50:30:10	10%
P3	2	10	7	4.4	10:43:29:18	18%
P4	2	10	7	6.6	8:40:26:26	26%
P5	2	10	7	8.8	7:36:25:32	32%
P6	2	10	7	11	7:34:23:36	36%

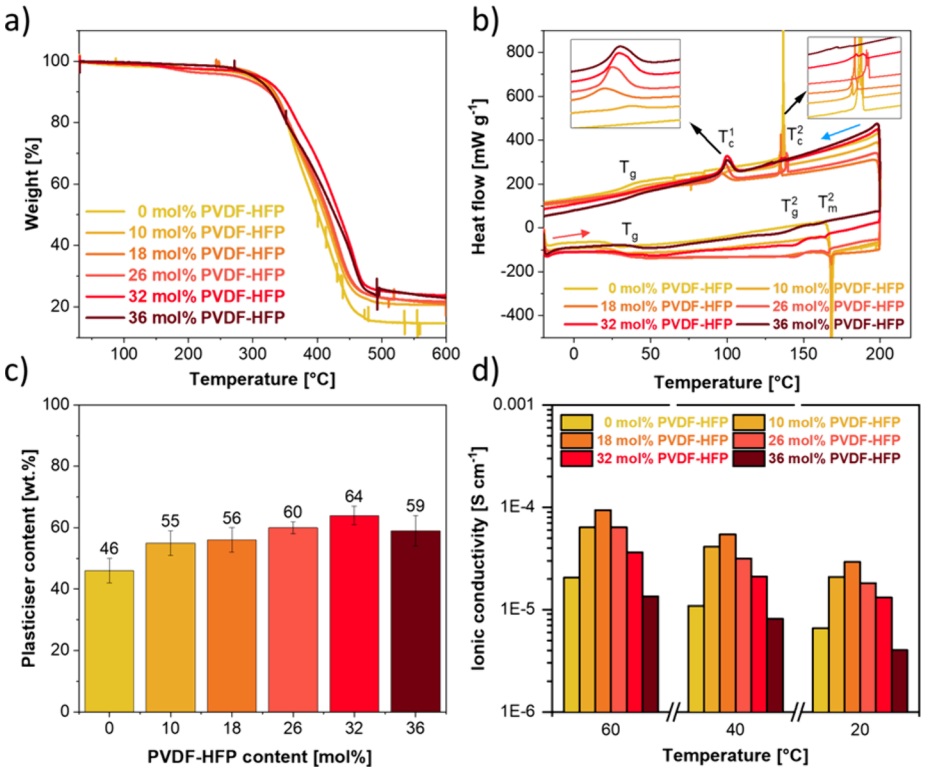

Figure 1. (a) TGA (heating rate of 5 K min^{-1}, inert He atmosphere), and (b) DSC (two cooling and heating cycles between −20 and 200 °C with a 5 K min^{-1} rate) of the dried NaSTFSI-SIPEs with different PVDF-HFP ratios from 2:10:7:0 (0% PVDF-HFP) to 2:10:7:11 (36 mol% PVDF-HFP). (c) Molecular transporter (EC:DMC:FEC in 49:49:2 vol. ratio) uptake in wt.% and (d) temperature-dependent ionic conductivity at 20, 40, and 60 °C of swelled NaSTFSI-SIPEs with different PVDF-HFP ratios from 0% PVDF-HFP to 36 mol% PVDF-HFP.

stabilization and electrochemical properties has been investigated. Theoretically, the best PET4A/PETMP mole ratio should be 1:1, allowing all functional groups of both backbone components to bind together without leaving any component unreacted. However, this ideal ratio changes when introducing the SSM, in this particular case, NaSTFSI, which has a free terminal double bond (vinyl group) to bind with a free thiol group of PETMP. Thus, the optimal amount of PET4A has to be slightly decreased so that PETMP can match all the vinyl groups of PET4A and SSM. In order to evaluate the best ratio of PET4A in relation to PETMP and NaSTFSI, PET4A/PETMP molar ratio has been varied between 40 and 100% (in 15% steps), while the molar ratio of NaSTFSI and PVDF-HFP vs PETMP was kept constant at 20% and 44%, respectively (see Table 1). This resulted in NaSTFSI-SIPE membranes with molar ratios ranging between 2:10:4:4.4 and 2:10:10:4.4 (NaSTFSI:PETMP:PET4A:PVDF-HFP), labeled as T1 to T5, respectively. From visual inspection, the optimal PET4A/PETMP molar ratio appears to be between 70 and 85% (Figure S3). Indeed, at low molar ratios (*i.e.*, T1: 40% and T2: 55%), the thiol groups of excess PETMP might be involved in side reactions, leading to a homopolymerization not forming a self-standing membrane. Meanwhile, high molar ratios (T5: 100%) result in the formation of subregions in the membrane, as the excess PET4A units yield side reactions. However, both the 2:10:7:4.4 (T3) and 2:10:8.5:4.4 (T4) (NaSTFSI:-PETMP:PET4A:PVDF-HFP) compositions result in self-standing membranes. Although both SIPE membranes visually look appropriate, the former (T3) is more homogeneous, less brittle, and more flexible. Additionally, more functional groups of PETMP are available for the SSM to connect with and were thus used for follow-up tests, where the SSM content was increased up to 24 mol%. Nevertheless, further optimization tests should be carried out in the range of 70−85% to identify the optimal SIPE composition, as well as mechanical studies to support the selection of the best composition.

Although the stability of the NaSTFSI-SIPE originates from the PET4A/PETMP backbone, it is additionally supported by PVDF-HFP. PVDF-HFP does not chemically bind to any of the components but improves the overall mechanical proper-

Table 3. Investigated SSM ratios in the dry NaSTFSI-SIPE membranes.

	molar ratio [mol]				composition [mol%]	investigated factor
SIPE label	NaSTFSI	PETMP	PET4A	PVDF-HFP	NaSTFSI:PETMP:PET4A:PVDF-HFP	molar% of NaSTFSI
M1	1	10	7	4.4	4:48:29:19	4%
M2	2	10	7	4.4	9:44:28:19	9%
M3	3	10	7	4.4	13:43:26:18	13%
M4	4	10	7	4.4	17:40:25:18	17%
M5	5	10	7	4.4	20:38:25:17	20%
M6	6	10	7	4.4	23:36:25:16	23%

ties upon the molecular solvent addition needed to increase the ionic conductivity of the electrolytic membrane. Taking constant the molar ratio of PET4A, PETMP, and NaSTFSI to 2:10:7, the number of PVDF-HFP units was varied between 0 and 11 (*i.e.*, from 2:10:7:0 to 2:10:7:11 in NaSTFSI:-PETMP:PET4A:PVDF-HFP). A total of six different compositions were explored, labeled as from P1 to P6 (Table 2).

PVDF-HFP did not negatively influence either the membrane stability or the homogeneity of the different SIPEs in the examined range (Figure S4). Therefore, the thermal and electrochemical stability of the six SIPE membranes with compositions between 2:10:7:0 (P1, 0% PVDF-HFP) and 2:10:7:11 (P6, 36 mol% PVDF-HFP) were evaluated to select the optimal composition.

The thermal stability was studied by TGA (Figure 1a) by heating the membranes up to 600 °C under He flow. All NaSTFSI-SIPE membranes are thermally stable up to 300 °C, which is comparable to other Na-based SIPEs.[18,37−39] The main difference between the various membranes is the increasing residual weight, which increases with increasing PVDF-HFP content. In addition, a DSC investigation has been carried out, involving heating from −20 up to 200 °C and cooling back to −20 °C (Figure 1b). The scan shows an increase in the heat flow at 40 °C for all SIPEs for the heating (lower) and cooling (upper) scans, which matches the glass transition temperature (T_g) observed for this specific type of PETMP/4A-based SIPE.[18] The NaSTFSI-SIPEs with molar compositions between 2:10:7:4.4 (P3, 18 mol% PVDF-HFP) and 2:10:7:11 (P6, 36 mol% PVDF-HFP) show a crystallization point at 100 °C (T_{c1}), which can be linked to the crystallization of PVDF-HFP chains (see the DSC of pure PVDF-HFP in Figure S5),[40] while the SIPEs with molar compositions between 2:10:7:0 (P1, 0% PVDF-HFP) and 2:10:7:8.8 (P5, 32 mol% PVDF-HFP) show a crystallization point at 140 °C (T_{c2}), which can be linked to the crystallization of the NaSTFSI-PET-MP/4A backbone. The intensity of the T_{c1} peak increases, while that of the T_{c2} peak decreases with an increasing PVDF-HFP content, suggesting that higher amounts of PVDF-HFP hinder the natural crystallization of the NaSTFSI-PET-MP/4A-PVDF-HFP SIPE backbone upon cooling, while PVDF-HFP chains crystallize once the amount is high enough to be completely enclosed or entangled inside the SIPE network.

In addition, during the heating cycle, the SIPE membranes with PVDF-HFP amounts between 0 and 18% show a melting point (T_{m2}) at 168 °C, which can be linked to the rearrangement of the NaSTFSI-PET-MP/4A polymer into a more stable and less crystalline structure. The NaSTFSI-SIPEs with ratios between 2:10:7:6.6 (P4, 26 mol% PVDF-HFP) and 2:10:7:11 (P6, 36 mol% PVDF-HFP) do not show this melting point, but instead indicate a second glass transition point (T_{g2}) at 140 °C, which can be linked to a reorganization of the NaSTFSI-PET-MP/4A polymer network. The intensity of both peaks is reduced with higher amounts of PVDF-HFP, as more PVDF-HFP results in narrower space, which creates a more amorphous structure and makes it even harder for the PETMP/4A network to crystallize, melt, or rearrange. Additionally, a high concentration of PVDF-HFP can result in the entanglement of PVDF-HFP chains with each other, which additionally could hinder the movement of the backbone during the heating (T_{g2}) and cooling (T_{c2}) cycles.[41−43]

The EC:DMC:FEC (49:49:2 vol.%) solvent mixture was incorporated as a molecular transporter into the NaSTFSI-SIPEs with a varying PVDF-HFP content to be used as electrolytes. The amount of the molecular transporter composition spontaneously uptaken by the different SIPEs was measured 3 times at 5 different positions of the membrane to provide a representative value (Figure 1c). The uptake varied between 45 and 65 wt.%. The relationship between the molecular transporter uptake and the PVDF-HFP content trend indicates a bell-shaped curve, with a maximum at 32 mol % PVDF-HFP. However, considering the larger error of the P6 (36 mol% PVDF-HFP), it might also be possible that this bell-shaped curve could represent a plateau, reflecting the maximum amount of molecular transporters that the SIPE can absorb, which is around 60 wt.%. Importantly, the amount of molecular transporter uptaken by the SIPE membranes influences the electrochemical properties, particularly ionic conductivity. This suggests that the first hypothesis of a bell-shaped trend is more plausible.[44,45] In fact, the ionic conductivity measured at 20, 40, and 60 °C (Figure 1d) supports this, as it also displays a bell-shaped trend at all temperatures, with an overall increase in ionic conductivity as temperature rises. This temperature range was chosen because most practical applications of solid-state batteries operate above room temperature. Therefore, 20−60 °C represents a relevant and realistic temperature range for these batteries. This trend can be explained by the DSC results, which are linked with the amount of PVDF-HFP and the concentration of SSM in the membrane. On the one hand, the amount of PVDF-HFP that can be inside the membrane without creating excess PVDF-HFP regions that disrupt the natural behavior of the polymer backbone (T_{c2} and T_{m2} still present) was found to be >18 mol% (from P3 to P6). On the other hand, the SSM concentration decreases with increasing PVDF-HFP content from P3 (10 mol%) to P6 (7 mol%). The lower amount of SSM results in a lower amount of Na^+, which leads to a decrease in ionic conductivity. Hence, P3 NaSTFSI-SIPE was selected due to the highest ionic conductivity at all temperatures, reaching a conductivity of 1×10^{-4} and 3×10^{-4} S cm^{-1} at 20 to 60 °C, respectively.

Finally, the amount of SSM has been investigated since it is crucial for ionic conductivity, as more anionic centers

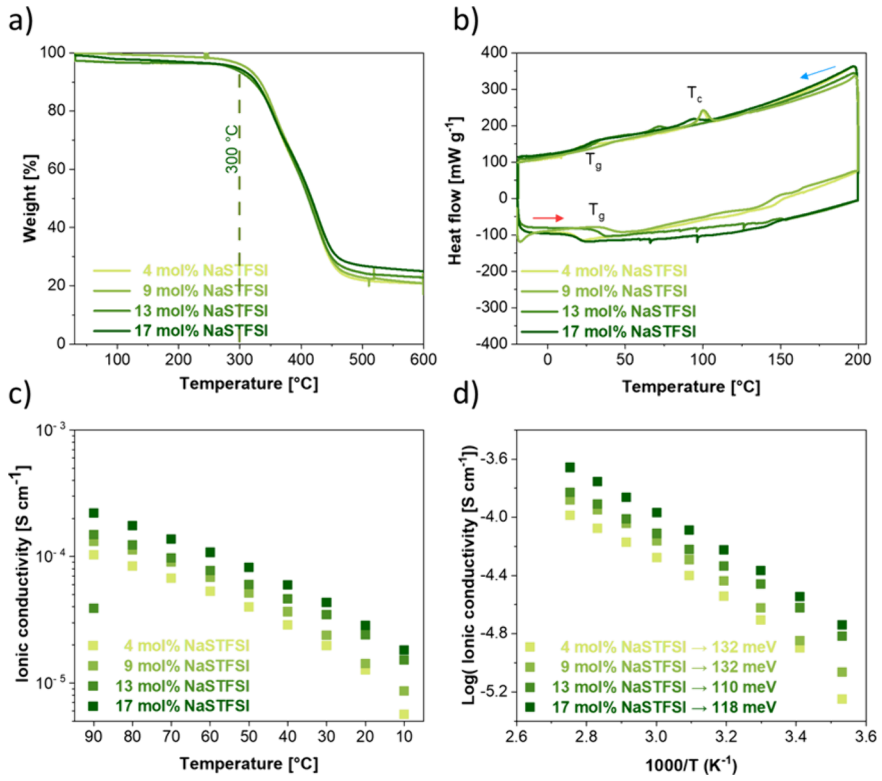

Figure 2. (a) TGA (heating rate of 5 K min^{-1}, inert He atmosphere), and (b) DSC (two cooling and heating cycles between −20 and 200 °C with a 5 K min^{-1} rate) of the dry NaSTFSI-SIPE with various SSM concentrations. (c) Temperature-dependent ionic conductivity and (d) activation energy of the NaSTFSI-SIPEs with different NaSTFSI contents (from 1:10:7:4.4 (M1) to 4:10:7:4.4 (M4)) and EC:DMC:FEC molecular transporter incorporation.

correspond to a larger number of Na^+ carriers as well as closer sites for charge transfer, facilitating the Na^+ transport. The effect of the NaSTFSI content in NaSTFSI-SIPE was studied by varying its content (Table 3) while maintaining the molar ratio for the other components (*x*:10:7:4.4, SSM:PETMP:PET4A:PVDF-HFP). The NaSTFSI-SIPEs with compositions between 1:10:7:4.4 (M1) and 4:10:7:4.4 (M4) were homogeneous and self-standing polymer membranes, while M5 and M6 showed inhomogeneities and cracks and were not considered as possible candidates due to concerns about reproducibility and scalability.

The observed inhomogeneities that occur in M5 and M6 (Figure S6) can be explained by unwanted side reactions that occur through the mismatch of too many vinyl groups in relation to thiol groups. The highest ratio of NaSTFSI that results in a homogeneous membrane consists of a ratio of 4:10:7:4.4 (M4), which means that 70% of the four thiol groups of each PETMP molecule are matched with PET4A vinyl groups, and 10% are matched with NaSTFSI vinyl groups. The remaining 20% of thiol groups are not bound to one of the other two monomers but face the supporting polymer PVDF-HFP, which has fluorine covering its surface, attracting the protons of the thiol groups.

The thermal and electrochemical properties of M1 (1:10:7:4.4) through M4 (4:10:7:4.4) NaSTFSI-SIPE self-standing membranes, incorporating around 50 wt.% of carbonate-based molecular transporters (for the electrochemical properties), were investigated. The TGA curve (Figure 2a) shows thermal stability up to 300 °C for all studied NaSTFSI-SIPE dry membranes, comparable with other Na-based SIPEs.[18,37−39] The different SIPE membranes show comparable thermal stabilities independent of the SSM content, suggesting that the monomer content does not influence the thermal stability of the SIPE and that all components are either chemically bonded or enclosed in the SIPE.

The DSC scan (Figure 2b) is in agreement with the TGA when heating from −20 °C up to 200 °C and back to −20 °C. The scan shows a T_g at 40 °C and a crystallization feature at 100 °C (T_{c1}), which can be linked to the crystallization of PVDF-HFP chains.[41]

The four SIPE membranes were further electrochemically characterized after the incorporation of EC:DMC:FEC (49:49:2 vol.%). First, the ionic conductivity of the NaSTFSI-SIPEs was tested at different temperatures between 10 and 90 °C (Figure 2c). The ionic conductivity increases with increasing temperature as commonly observed for SIPEs.[44,45] More interestingly, the conductivity increases with an increasing NaSTFSI content, reaching a maximum of 2.2×10^{-4} S cm^{-1} at 90 °C for the membrane with the 4:10:7:4.4 composition (M4, 17 mol% NaSTFSI). This trend supports the assumption that more anionic centers result in a higher number of Na^+ charge carriers and a shorter distance that each Na^+ has to travel between two anionic centers. The activation energy for Na^+ transport (Figure 2d) in the investigated temperature range is between 132 and 118 meV for the M1 to M4 SIPEs with a tendency toward lower activation energy with a higher number of Na^+ carriers, most likely due to the closer proximity of the anionic centers.

Considering the previous results, the NaSTFSI-SIPE with the 4:10:7:4.4 mol composition (M4, 17 mol% NaSTFSI), which shows the highest conductivity, as well as the 2:10:7:4.4

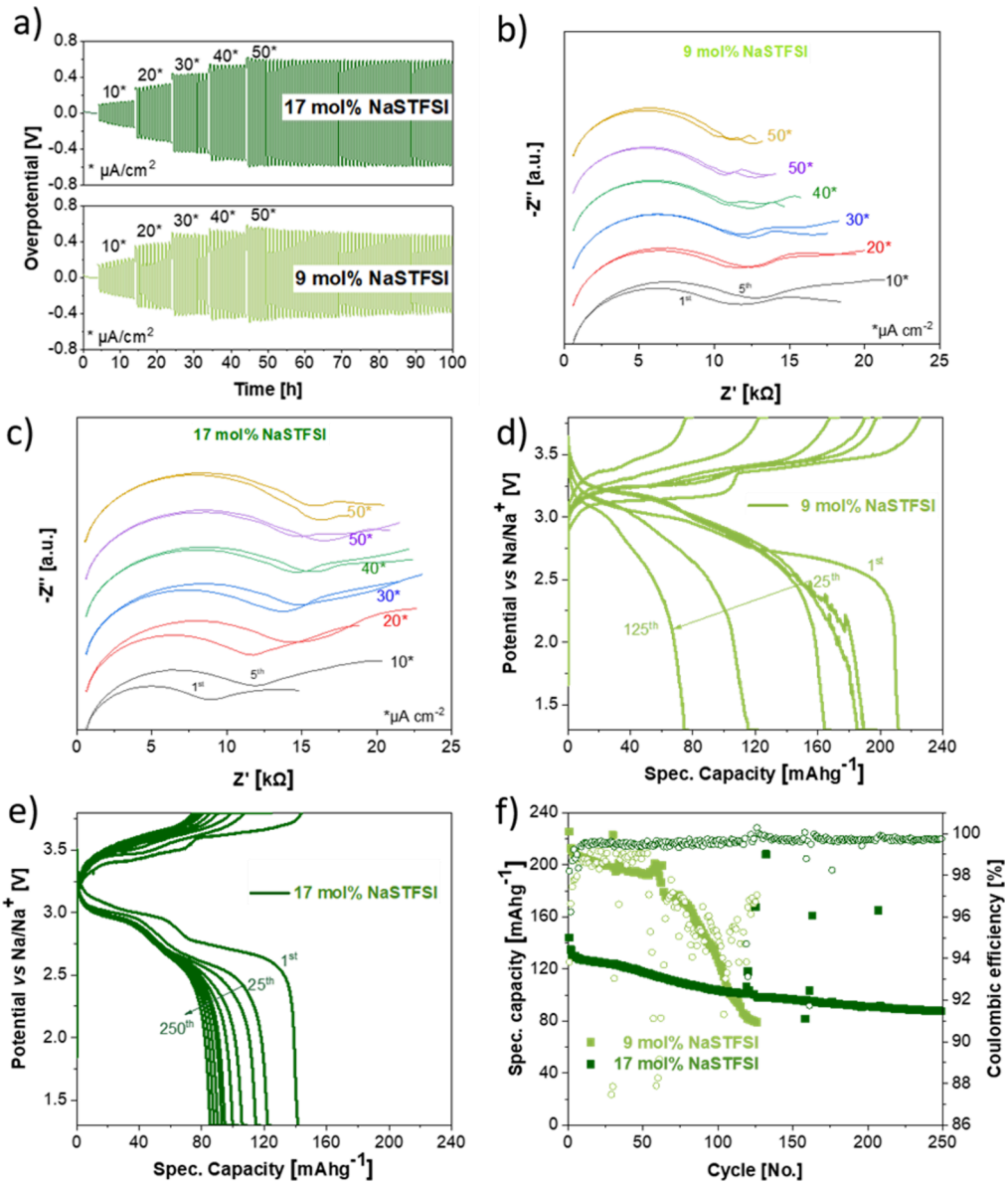

Figure 3. (a) Na stripping/plating tests of Na||M2||Na and Na||M4||Na cells at different current densities at 40 °C. Nyquist plots after the initial and last cycles at different current densities if (b) the Na||M2||Na and (c) the Na||M4||Na cell. Voltage profiles of Na||NaSTFSI-SIPE||PW cells composed (d) 2:10:7:4.4 (9 mol% NaSTFSI, light green) and (e) 4:10:7:4.4 (17 mol% NaSTFSI, dark green), and (f) the corresponding specific capacity and Coulombic efficiency upon cycling. EC:DMC:FEC (49:49:2 vol .%) molecular transporter is incorporated into all SIPEs. The galvanostatic cycling test with a current density of 0.02C in the first cycle, followed by 5 cycles at 0.05C and ongoing ones at 0.1C between 3.8 and 1.3 V vs Na^+/Na. All measurements were performed at 40 °C.

mol composition (M2, 9 mol% NaSTFSI), having the composition comparable to the previously published SIPE,[18] have been implemented in symmetric Na||Na cells to examine the Na stripping/plating behavior, the stability against Na metal and the SEI formation upon cycling (Figure 3a). Both NaSTFI-SIPEs show stable cycling up to 50 μA cm^{-2} with no visible increase in overpotential. However, the overpotential of M2 (2:10:7:4.4) decreases upon continuous cycling at 50 μA cm^{-2}, stabilizing around 0.46 V. Meanwhile, the overpotential of M4 (4:10:7:4.4) remains stable at 0.58 V. Impedance analysis has been conducted to identify potential differences in SEI formation. Figure 3b,c displays the Nyquist plots of Na cells using M2 and M4 as electrolytes, respectively, after the first and last cycles at each applied current density. The M2-containing cell exhibits slightly lower overall resistance compared to M4 cells. In the case of M2, the resistance decreases upon cycling and increasing the current density. In contrast, the M4-based cell shows higher overall resistance, which increases during the initial cycles and at low currents but remains constant after applying 40 μA cm^{-2}. These results align with the trends observed in overpotential, suggesting that the higher fluorine content in M4 led to the formation of a thicker NaF-rich interphase, as previously investigated in our group,[18] due to the reactivity with the surface of Na metal. In addition, the increased resistance associated with NaF may contribute to the higher overpotential seen in M4 cells, such as LiF.[46] In the case of the M2-based cell, the decreasing overpotential suggests that the SEI is decomposing upon cycling and is likely unstable, potentially due to a lower NaF

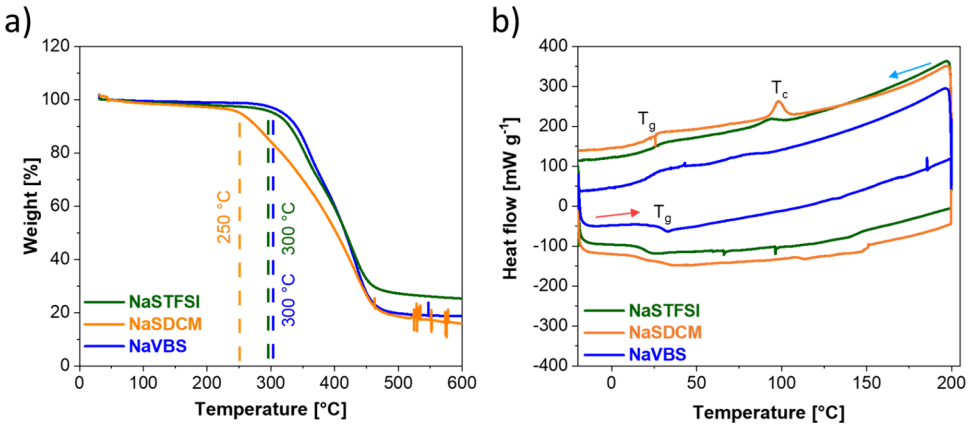

Figure 4. (a) TGA (heating rate of 5 K min^{-1}, inert He atmosphere) and (b) DSC (cooling and heating cycles between −20 and 200 °C with a 5 K min^{-1} rate) of the dried NaSTFSI-, NaSDCM-, and NaVBS-SIPEs with the 4:10:7:4.4 molar composition.

formation, which is highly soluble in carbonate molecular transporters (3.057 mg L^{-1}).[47]

The M2 and M4 NaSTFSI-SIPE were investigated in quasi-solid-state Na-metal cells employing PW as a cathode as a proof of concept. The voltage profiles of Na||PW cells, using both SIPEs, are shown in Figure 3d,e, respectively. The initial charge and discharge capacities of the cell employing M4 at 0.02C are 144 and 141 mAh g^{-1}, respectively, while those of the cell containing M2 are 225 and 211 mAh g^{-1}, respectively. The Na||PW cell with M4 shows higher cell polarization and, thus, lower initial specific capacity compared to the cell with M2, which is in agreement with the stripping/plating tests. The lower polarization of the cell employing M2, on the other hand, results in a higher initial delivered specific capacity. In addition, the delivered specific capacity of the cell containing M2 is higher than the theoretical capacity of the PW (150 mAh g^{-1}), suggesting that the extra capacity is due to the contribution of side reactions, which agrees with the rapid capacity decay and poor Coulombic efficiency. Meanwhile, the voltage profile of the M4-based PW cell is rather stable upon cycling, showing the two characteristic plateaus of PW at 3.0 and 3.3 V vs Na^+/Na.

As already mentioned, the specific capacity upon long-term cycling test (Figure 3f) shows that the Na||PW cell employing M2 delivers an initially higher specific capacity than the M4-based cell (200 mAh g^{-1} vs 125 mAh g^{-1}). However, the electrochemical performance of the former cell exhibits a fast and continuous fading, reaching 80 mAh g^{-1} after 120 cycles. Meanwhile, the Na||M4||PW cell shows more stable capacity, resulting in a longer-term cycling performance, delivering a specific capacity of 100 mAh g^{-1} after 120 cycles at 40 °C. The cycling performance is in line with the Coulombic efficiency values. The M2-based cell shows an initial Coulombic efficiency of 93.8%, which increases up to 98.8% in the following 50−60 cycles, but then it drops down to 94% upon cycling, suggesting once more the occurrence of side reactions and electrolyte decomposition, as well as Na dendrite formation. In contrast, the cell with M4 exhibits an initial Coulombic efficiency of 98.2% that stabilizes around 99.9%. The highest stability upon cycling and the most stable overpotential upon stripping/plating support for the M4-based SIPE to have a more homogeneous and stable SEI compared to the M2-based SIPE and to have the best chemical composition among all investigated SIPEs.

Influence of the SSM Anionic Center on the SSM-PET-MP/4A-PVDF-HFP-Based SIPEs. Various SSMs carrying Na^+ were synthesized to produce different SIPEs for sodium-based batteries. The mobility of Na cations inversely depends on the binding strength toward the anion, which is tethered to the backbone and is thus referred to as the anionic center. Increasing the anionic center size increases the delocalization of the negative charge, resulting in a weaker interaction between the anion and the cation, in turn improving the Na^+ conductivity.

The effect of the anionic center's charge delocalization on the SIPE performance has been investigated using NaSTFSI, NaSDCM, or NaVBS SSMs (Figure S7) in SSM-PET-MP/4A-PVDF-HFP-based SIPE with the mol composition 4:10:7:4.4 (optimized from the section above). The three SSMs have anionic centers attached to a benzene ring containing a vinyl group in para-position, which is used to build a chemical connection to the polymer backbone. However, NaSTFSI comprises a TFSI- group that widely delocalizes the negative charge on a nitrogen atom *via* two $-SO_2-$ groups, as well as a neighbored electron-drawing $-CF_3$ group. Meanwhile, NaSDCM carries the negative charge on a carbon atom that has two neighboring −CN- groups to delocalize the charge, and NaVBS carries the negative charge on an oxygen atom that is attached to the $-SO_2-$ group.

The thermal stability of the SIPE membranes incorporating the three SSMs was investigated by TGA measurements (Figure 4a). Each SIPE membrane is labeled by its containing SSM in the following. The NaSTFSI- and NaVBS-based SIPEs remain thermally stable up to 300 °C, while the NaSDCM-based SIPE membrane shows slightly lower thermal stability (up to 250 °C). This reduced thermal stability can be linked to the C−CN bonds of the SDCM monomer.[48] The DSC measurements (Figure 4b) show a T_g at 40 °C for all samples and a T_c at around 100 °C for the NaSTFSI and NaSDCM-based SIPEs. The absence of a visible crystallization peak for the NaVBS-based SIPE indicates that the crystalline content of the polymer is smaller compared to the other SIPEs upon cooling. This can be explained by the small, unshielded negative $-SO_3$ group, which has a stronger repulsive force against the PVDF-HFP chains and against itself compared to the other two SSMs. This increased repulsive force reduces the degree of crystallinity by hindering the formation of a semicrystalline orientation of the membrane, thus resulting in the absence of the crystallization peak.

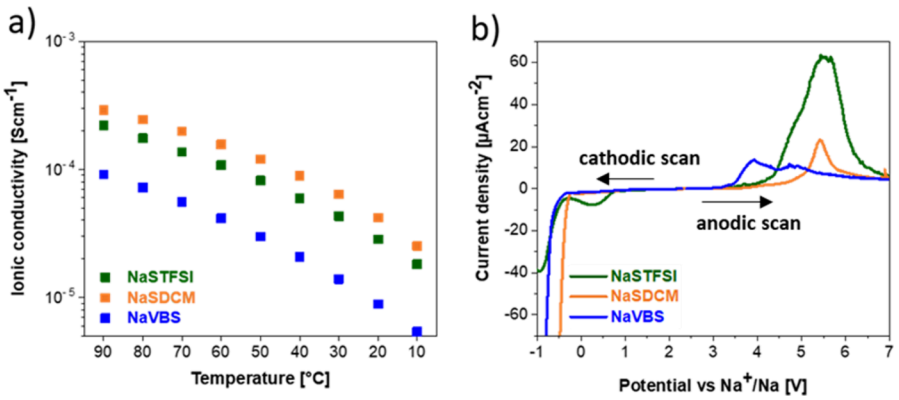

Figure 5. (a) Temperature-dependent ionic conductivity and (b) anodic and cathodic stability LSV curves (Al||SIPE||Na, scan rate of 30 μV s^{-1}, temperature 40 °C) of the NaSTFSI-, NaSDCM-, or NaVBs-SIPE with 50 wt.% of carbonate-based molecular transporters.

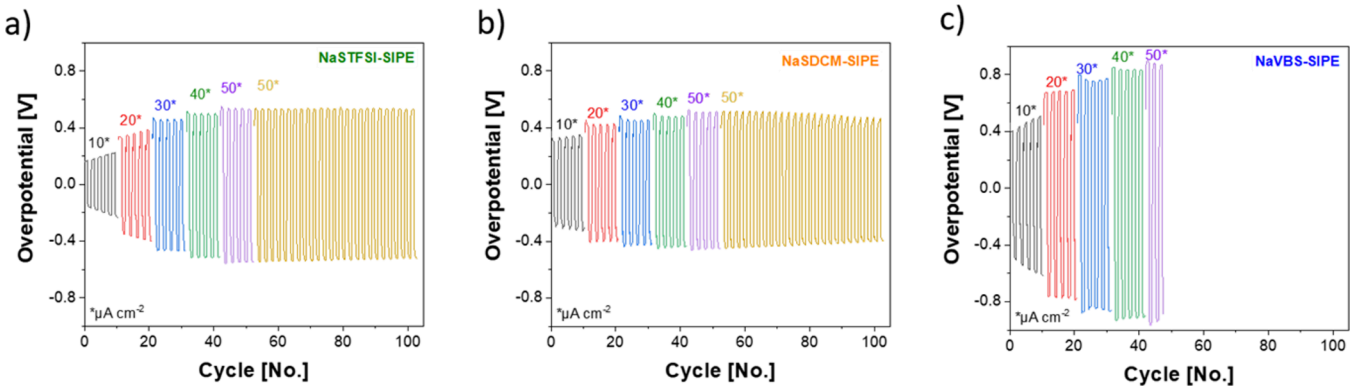

Figure 6. Na stripping/platting tests at different current density of (a) NaSTFSI-SIPE, (b) NaSDCM-SIPE, and (c) NaVBS-SIPE at 40 °C with carbonate-based molecular transporter (EC:DMC:FEC, 49:49:2 vol.%) .

The ionic conductivity of the three SIPEs with 50 wt.% of molecular transporters was studied between 10 and 90 °C. The measurement was performed in two sweeps, starting at 20 °C and increasing to 90 °C, followed by cooling to 10 °C. All SIPEs show their capability to transport Na^+ and reach ionic conductivities comparable to other SIPEs blended with PVDF-HFP.[38,39,45] The ionic conductivity (Figure 5a) results reveal that the NaVBS-SIPE shows the lowest conductivity with 8.9×10^{-6} S cm^{-1} at RT (9.1×10^{-5} at 90 °C), followed by NaSTFSI-SIPE, which reaches a conductivity of 2.84×10^{-5} S cm^{-1} at RT (2.2×10^{-4} at 90 °C), and NaSDCM-SIPE, which displays the highest conductivity of 4.2×10^{-5} S cm^{-1} at RT (2.9×10^{-4} at 90 °C), slightly higher to those observed in dry dual-ion SPEs and comparable with other Na-based SIPE.[38,39,45,49,50] These values match with the charge delocalization, *i.e.*, dissociation energy, of the various SSMs, with NaVBS having the weakest charge delocalization, *i.e.*, the highest required dissociation energy and the lowest conductivity. On the other hand, NaSDCM has the lowest dissociation energy and the highest conductivity. This result clearly demonstrates the importance of the dissociation energy on the ionic conductivity of SIPE, making it an essential parameter to consider when designing a SSM.

The electrochemical stability window of the different SIPEs has been investigated by LSV (Figure 5b). All of them do not show any limitation on the cathodic side prior to Na plating below 0 V vs Na^+/Na. Only the NaSTFSI-SIPE displays a fragment at 0.25 V, which might be related to the remaining DMSO inside the SIPE. The current flowing during the anodic scan is higher for NaSTFSI- compared to NaSDCM- and NaVBS-SIPEs, which suggests that the NaSTFSI-based SIPE oxidizes faster than those consisting of NaSDCM or NaVSBs. More important, however, is the onset potential for electrolyte oxidation, which is the lowest for NaVBS and the highest for NaSDCM. The former SIPE exhibits the current onset slightly above 3.0 V vs Na^+/Na, suggesting a high reactivity of the $-SO_3$ group. The NaSDCM-SIPE instead shows rather high anodic stability with no current flowing below 4.5 V vs Na^+/Na. Finally, NaSTFSI shows the anodic current flow starting at 4.0 V vs Na^+/Na. These results support the highest resistance of the DCM anionic center (and the SIPE) toward oxidation, which combines well with its highest conductivity.

To further characterize the SIPEs, stripping and plating tests were performed in Na||Na symmetric cells (Figure 6), which showed an increase in the overpotential for all SIPEs when the current was increased from 10 to 50 μA cm^{-2}. The NaSTFSI-SIPE exhibits an initial overpotential of 0.3 V vs Na^+/Na at 10 μA cm^{-2}, which increases with increasing current density to 0.52 V at 50 μA cm^{-2}. Meanwhile, the NaSDCM-SIPE displays a similar initial overpotential of 0.3 V at 10 μA cm^{-2}, which is slightly lower than NaSTFSI-SIPE upon cycling and increasing the current (*e.g.*, 0.45 V). Moreover, the overpotential remains constant and slightly decreases upon cycling, suggesting that NaSDCM-SIPE exhibits a thinner and/or less resistive SEI and thus represents a better choice as an electrolyte for Na-metal cells. Finally, the NaVBS-SIPE exhibits an initial overpotential of more than 0.4 V, which increases to 0.85 V at 50 μA cm^{-2}, indicating that this electrolyte cannot support high current

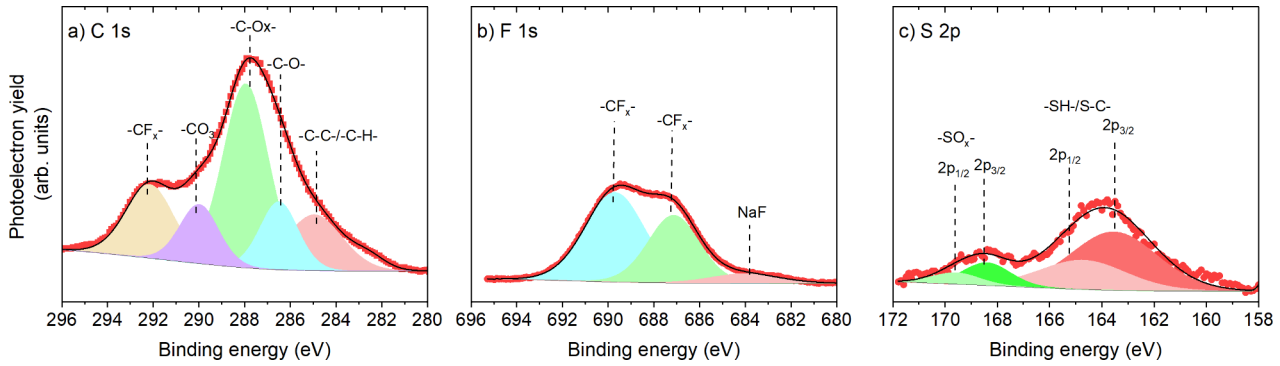

Figure 7. XPS analysis of NaSDCM-SIPE SEI. High-resolution (a) C 1s, (b) F 1s, and (c) S 2p photoelectron regions.

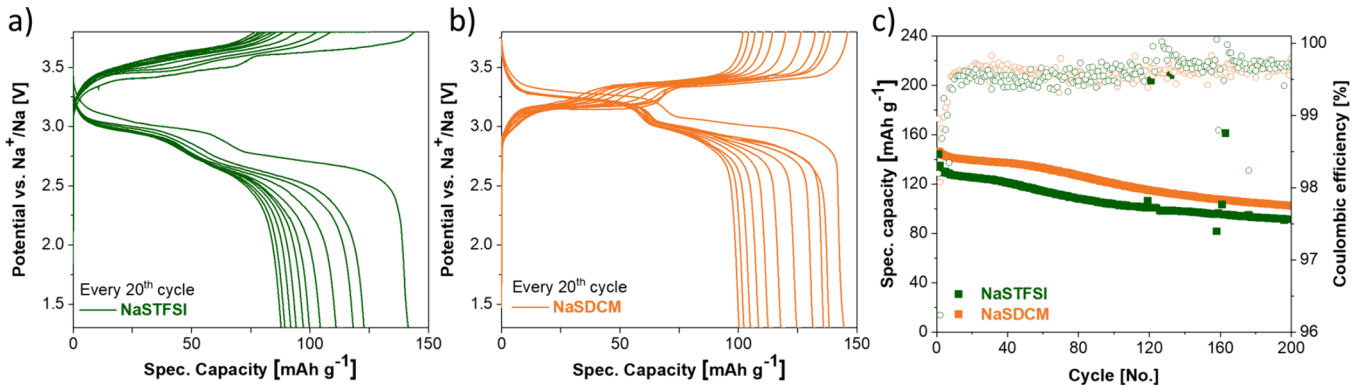

Figure 8. Voltage profiles of Na||SIPE||PW cells composed of (a) NaSTFSI- and (b) NaSDCM-SSMs and (c) the corresponding specific capacity and Coulombic efficiency upon cycling. EC:DMC:FEC (49:49:2 vol.%) molecular transporter is incorporated into all SIPEs. The galvanostatic cycling test with a current density of 0.02C the 1st cycle, followed by 5 cycles at 0.05C and ongoing ones at 0.1C between 3.8 and 1.3 V. All measurements were performed at 40 °C.

densities and, therefore, was excluded from subsequent experiments.

The slightly lower overpotential observed for NaSDCM-SIPE when cycled at 50 μA cm^{-2} may be related to the formation of a thinner and less resistive SEI. Therefore, *ex-situ* XPS analysis was conducted to compare the SEI chemistry formed on the surface of NaSDCM-SIPE with that formed on NaSTFSI-SIPE after cycling Na||Na symmetric cells. Figure 7 displays the high-resolution C 1s, F 1s, and S 2p photoelectron regions for NaSDCM-SIPE, while Figure S8 shows the corresponding regions for NaSTFSI-SIPE. The C 1s spectrum reveals five main species: hydrocarbons (C−C at 285.0 eV), carbon−oxygen species, including ether-based (C−O at ∼286 eV) ,and −CO$_x$− species (287 eV), carbonates (−CO$_3$ at ∼290 eV), and carbon−fluorine-containing compounds (−CF$_x$ at ∼291 eV).[36,51] These species are indicative of the molecular transporter mixture and its reduction products,[52] consistent with those detected for NaSTFSI-SIPE.[18] Notably, the F 1s spectrum shows that the fluorine-containing species undergo dehydrofluorination, resulting in the formation of NaF (684 eV).[18,53,54] However, the degradation of these species to form NaF is less pronounced in NaSDCM-SIPE compared to NaSTFSI-SIPE, suggesting a lower degree of decomposition and a thinner SEI. The main peaks in this region are associated with C−F species originating from PVDF-HFP.[51] Similarly, the S 2p spectrum indicates that the primary compound is SIPE (S−H/S−C at ∼164 eV), with a lower concentration of −SO$_x$− (∼169 eV) species observed, contrasting with the findings for NaSTFSI-SIPE. These results demonstrate that NaSDCM is more stable against Na metal than NaSTFSI-SIPE, leading to the formation of a thinner SEI that results in a lower overpotential and a less resistive interphase.

The NaSTFSI-based and NaSDCM-based SIPEs were used to realize proof-of-concept Na||SIPE||PW cells, while the NaVBS-SIPE was excluded from subsequent experiments, considering it exhibits a low ionic conductivity and poor oxidation stability not being compatible with PW cathode material.

The voltage profiles of Na||NaSTFSI-SIPE||PW (Figure 8a) cell show first cycle charge and discharge capacity of 144 and 141 mAh g^{-1} at 0.02C, respectively. Meanwhile, the Na||NaSDCM-SIPE||PW (Figure 8b) cell shows an initial charge and discharge capacity of 146 and 145 mAh g^{-1} at 0.02C, respectively. With both SIPEs, the cells exhibit two plateaus (more defined for the NaSDCM-SIPE-based cell) at 3.0 and 3.3 V vs Na$^+$/Na. However, the cell containing NaSTFSI-SIPE shows higher polarization and lower specific capacity.

The specific capacity of the cells decays when increasing the current from 0.02C to 0.05C and 0.1C, independent of the used SIPE. The specific capacity of the cell with NaSTFSI-SIPE reaches 91 mAh g^{-1} after 200 cycles, while that employing NaSDCM-SIPE still delivers 102 mAh g^{-1} after 200 cycles (Figure 8c). Nonetheless, the average Coulombic efficiency is above 99% for both SIPEs, suggesting that both SIPEs can be considered good candidates to be implemented in the quasi-solid-state Na cells. The NaSTFSI-SIPE-containing cell shows a slightly higher initial capacity drop, as well as capacity jumps upon cycling, due to dendrite formations. However, a more stable initial capacity for the cells

with NaSDCM-SIPE might be related to the formation of a more stable and/or thinner SEI compared to the NaSTFSI analog due to the absence of fluorine in the SSM that reduces the formation of NaF by reacting with the Na metal, as confirmed the XPS results.[18]

CONCLUSIONS

The component-driven effects on the thermal and electrochemical properties of SSM-PET-MP/4-PVDF-HFP SIPE have been investigated. The PETMP/PET4A ratio of 10 to 7 has been found to yield the highest homogeneity and was, thus, further used for subsequent optimization. The PVDF-HFP content was also explored by investigating molar ratios between 2:10:7:0 and 2:10:7:11 (NaSTFSI: PETMP:PET4A:PVDF-HFP). The 2:10:7:4.4 was determined to be the one offering the best ionic conductivity. Next, the SSM quantities were assessed using NaSTFSI as the exemplary SSM in the molar ratios between 1:10:7:4.4 and 6:10:7:4.4 (NaSTFSI: PETMP:PET4A:PVDF-HFP). The 4:10:7:4.4 molar ratio (NaSTFSI: PETMP:PET4A:PVDF-HFP) showed the highest ionic conductivity and the best cycling performance, in terms of capacity, Coulombic efficiency and long-term cycling (100 mAh g^{-1} after 120 cycles with a Coulombic efficiency of 99.9%). Higher SSM ratios resulted in unstable membranes, and lower ratios resulted in poorer conductivity. Last, the impact of the SSM anionic center on the electrochemical performance of the SIPE was examined using either NaSTFSI, NaSDCM, or NaVBS as SSMs. The large NaSDCM and NaSTFSI groups, owning stronger charge delocalization effects, and for NaSDCM also a low dissociation energy, resulted in higher conductivity compared to NaVBS. Overall, the NaSDCM-based SIPE showed the best performance with a conductivity of 4.2×10^{-5} S cm^{-1} at RT and 2.9×10^{-4} S cm^{-1} at 90 °C, a thermal stability of up to 300 °C, and an electrochemical stability window between 0 and almost 5 V vs Na^+/Na. Furthermore, Na||SIPE||PW cells employing such a SIPE delivered a specific capacity of 102 mAh g^{-1} after 200 cycles at 0.1C and 40 °C, showing the potential of such an optimized SIPE in Na-metal batteries but also indicating the need for further optimization to develop further advanced SIPEs for SMBs/ZESMBs.

AUTHOR INFORMATION

Corresponding Authors

Maider Zarrabeitia − *Helmholtz Institute Ulm (HIU), Ulm 89081, Germany; Karlsruhe Institute of Technology (KIT), Karlsruhe 76021, Germany;* orcid.org/0000-0003-1305-2136; Email: maider.ipina@kit.edu

Stefano Passerini − *Helmholtz Institute Ulm (HIU), Ulm 89081, Germany; Karlsruhe Institute of Technology (KIT), Karlsruhe 76021, Germany;* Present Address: Austrian Institute of Technology (AIT), Center for Transport Technologies, Giefinggasse 2, 1220 Wien, Austria (S.P.); orcid.org/0000-0002-6606-5304; Email: stefano.passerini@kit.edu

Authors

Clemens Wunder − *Helmholtz Institute Ulm (HIU), Ulm 89081, Germany; Karlsruhe Institute of Technology (KIT), Karlsruhe 76021, Germany*

Leo Graeber − *Helmholtz Institute Ulm (HIU), Ulm 89081, Germany; Karlsruhe Institute of Technology (KIT), Karlsruhe 76021, Germany*

Dominic Bresser − *Helmholtz Institute Ulm (HIU), Ulm 89081, Germany; Karlsruhe Institute of Technology (KIT), Karlsruhe 76021, Germany;* orcid.org/0000-0001-6429-6048

Author Contributions

C.W. performed investigation, methodology, data analysis, visualization, writing—original draft and editing. L.G. performed a synthesis of the NaSDCM SSM. D.B. performed supervision, review, and editing. M.Z. performed conceptualization, methodology, investigation, formal analysis, project administration, supervision, writing-review, and editing. S.P. performed conceptualization, methodology, funding acquisition, supervision, and writing—review and editing.

Funding

HORIZON 2020 program (Project "S IMBA" 963542) and Helmholtz Association.

Notes

The authors declare no competing financial interest.

ACKNOWLEDGMENTS

This work was funded by the HORIZON 2020 program (Project "SIMBA" 963542). The authors thank the Helmholtz Association for the financial support. The von Delius group at Ulm University is acknowledged for the solution NMR measurements, and Altris AB for providing the Prussian White cathode material.

REFERENCES

(1) Qiao, L.; Judez, X.; Rojo, T.; Armand, M.; Zhang, H. Review—Polymer Electrolytes for Sodium Batteries. *J. Electrochem. Soc.* **2020**, *167*, No. 070534.

(2) Zhang, H.; Li, C.; Eshetu, G. G.; Laruelle, S.; Grugeon, S.; Zaghib, K.; Julien, C.; Mauger, A.; Guyomard, D.; Rojo, T.; Gisbert-Trejo, N.; Passerini, S.; Huang, X.; Zhou, Z.; Johansson, P.; Forsyth, M. From Solid-Solution Electrodes and the Rocking-Chair Concept to Today's Batteries. *Angew. Chem.* **2020**, *132*, 542−546.

(3) International Energy Agency *Critical Minerals* https://www.iea.org/, 2025.

(4) Chu, S.; Majumdar, A. Opportunities and challenges for a sustainable energy future. *Nature* **2012**, *488*, 294−303.

(5) Zhao, C.; Liu, L.; Qi, X.; Lu, Y.; Wu, F.; Zhao, J.; Yu, Y.; Hu, Y.-S.; Chen, L. Solid-State Sodium Batteries. *Adv. Energy Mater.* **2018**, *8*, No. 1703012.

(6) Chayambuka, K.; Mulder, G.; Danilov, D. L.; Notten, P. H. L. Sodium-Ion Battery Materials and Electrochemical Properties Reviewed. *Adv. Energy Mater.* **2018**, *8*, No. 1800079.
(7) Hasa, I.; Mariyappan, S.; Saurel, D.; Adelhelm, P.; Koposov, A. Y.; Masquelier, C.; Croguennec, L.; Casas-Cabanas, M. Challenges of today for Na-based batteries of the future: From materials to cell metrics. *J. Power Sources* **2021**, *482*, No. 228872.
(8) Nayak, P. K.; Yang, L.; Brehm, W.; Adelhelm, P. From Lithium-Ion to Sodium-Ion Batteries: Advantages, Challenges, and Surprises. *Angew. Chem., Int. Ed.* **2018**, *57*, 102−120.
(9) Peters, J.; Peña Cruz, A.; Weil, M. Exploring the Economic Potential of Sodium-Ion Batteries. *Batteries* **2019**, *5*, 10.
(10) Wang, Y.; Song, S.; Xu, C.; Hu, N.; Molenda, J.; Lu, L. Development of solid-state electrolytes for sodium-ion battery − A short review. *Nano Mater. Sci.* **2019**, *1*, 91−100.
(11) Zeng, R. *CATL Unveils Its Latest Breakthrough Technology by Releasing Its First Generation of Sodium-ion Batteries*, CATL https://www.catl.com/en/news/665.html (2021).
(12) Swallow, T. *CATL leads EV battery production and SIBs have its attention*. EV Magazine https://evmagazine.com/charging-and-infrastructure/catl-leads-ev-battery-production-and-sibs-have-its-attention (2023).
(13) Power Technology, *BYD breaks ground on new 30GWh sodium-ion battery facility in China* https://www.power-technology.com/news/byd-sodium-battery-facility-china/ (2024).
(14) Barker, J.; Heap, R. J.; Roche, N.; Tan, C.; Sayers, R.; Whitley, J.; Lui, Y. *Commercialization of Faradion's High Energy Density Na-ion Battery Technology*. Faradion https://faradion.co.uk/wp-content/uploads/2018/04/Faradion-Limited-3rd-International-Meeting-on-Sodium-Batteries.pdf (2018).
(15) Rudola, A.; Rennie, A. J. R.; Heap, R.; Meysami, S. S.; Lowbridge, A.; Mazzali, F.; Sayers, R.; Wright, C. J.; Barker, J. Commercialization of high energy density sodium-ion batteries: Faradion's journey and outlook. *J. Mater. Chem. A* **2021**, *9*, 8279−8302.
(16) Ghazi, Z. A.; Sun, Z.; Sun, C.; Qi, F.; An, B.; Li, F.; Cheng, H.-M. Key Aspects of Lithium Metal Anodes for Lithium Metal Batteries. *Small* **2019**, *15*, No. 1900687.
(17) Yang, T.; Luo, D.; Liu, Y.; Yu, A.; Chen, Z. Anode-free sodium metal batteries as rising stars for lithium-ion alternatives. *iScience* **2023**, *26*, No. 105982.
(18) Wunder, C.; Lai, T.-L.; Sic, E.; Gutmann, T.; De Vito, E.; Buntkosky, G.; Zarrabeitia, M.; Passerini, S. Sodium 4-styrenesulfonyl-(trifluoromethanesulfonyl)imide-based single-ion conducting polymer electrolyte incorporating molecular transporters for quasi-solid-state sodium batteries. *J. Mater. Chem. A* **2024**, *12*, 20935−20946.
(19) Han, J. Y.; Jung, S. Thermal Stability and the Effect of Water on Hydrogen Fluoride Generation in Lithium-Ion Battery Electrolytes Containing $LiPF_6$. *Batteries* **2022**, *8*, 61.
(20) McOwen, D. W.; Seo, D. M.; Borodin, O.; Vatamanu, J.; Boyle, P. D.; Henderson, W. A. Concentrated electrolytes: decrypting electrolyte properties and reassessing Al corrosion mechanisms. *Energy Env. Sci.* **2014**, *7*, 416−426.
(21) Liu, Q.; Geng, Z.; Han, C.; Fu, Y.; Li, S.; He, Y-b; Kang, F.; Li, B. Challenges and perspectives of garnet solid electrolytes for all solid-state lithium batteries. *J. Power Sources* **2018**, *389*, 120−134.
(22) Xi, G.; Xiao, M.; Wang, S.; Han, D.; Li, Y.; Meng, Y. Polymer-Based Solid Electrolytes: Material Selection, Design, and Application. *Adv. Funct. Mater.* **2021**, *31*, No. 2007598.
(23) Fergus, J. W. Ceramic and polymeric solid electrolytes for lithium-ion batteries. *J. Power Sources* **2010**, *195*, 4554−4569.
(24) Eshetu, G. G.; Elia, G. A.; Armand, M.; Forsyth, M.; Komaba, S.; Rojo, T.; Passerini, S. Electrolytes and Interphases in Sodium-Based Rechargeable Batteries: Recent Advances and Perspectives. *Adv. Energy Mater.* **2020**, *10*, No. 2000093.
(25) Yang, J.; Zhang, H.; Zhou, Q.; Qu, H.; Dong, T.; Zhang, M.; Tang, B.; Zhang, J.; Cui, G. Safety-Enhanced Polymer Electrolytes for Sodium Batteries: Recent Progress and Perspectives. *ACS Appl. Mater. Interfaces* **2019**, *11*, 17109−17127.
(26) Genix, A.-C.; et al. Enhancing the Mechanical Properties of Glassy Nanocomposites by Tuning Polymer Molecular Weight. *ACS Appl. Mater. Interfaces* **2018**, *10*, 33601−33610.
(27) South, C. R.; Burd, C.; Weck, M. Modular and Dynamic Functionalization of Polymeric Scaffolds. *Acc. Chem. Res.* **2007**, *40*, 63−74.
(28) Deng, L.; Chen, G. Recent progress in tuning polymer oriented microstructures for enhanced thermoelectric performance. *Nano Energy* **2021**, *80*, No. 105448.
(29) Wojtecki, R. J.; Nelson, A. Small changes with big effects: Tuning polymer properties with supramolecular interactions. *J. Polym. Sci. Part Polym. Chem.* **2016**, *54*, 457−472.
(30) Papananou, H.; Perivolari, E.; Chrissopoulou, K.; Anastasiadis, S. H. Tuning polymer crystallinity via the appropriate selection of inorganic nanoadditives. *Polymer* **2018**, *157*, 111−121.
(31) Chen, L.; Xu, S.; McBranch, D.; Whitten, D. Tuning the Properties of Conjugated Polyelectrolytes through Surfactant Complexation. *J. Am. Chem. Soc.* **2000**, *122*, 9302−9303.
(32) Bubnova, O.; Berggren, M.; Crispin, X. Tuning the Thermoelectric Properties of Conducting Polymers in an Electrochemical Transistor. *J. Am. Chem. Soc.* **2012**, *134*, 16456−16459.
(33) Zhang, H.; Li, C.; Piszcz, M.; Coya, E.; Rojo, T.; Rodriguez-Martinez, L. M.; Armand, M.; Zhou, Z. Single lithium-ion conducting solid polymer electrolytes: advances and perspectives. *Chem. Soc. Rev.* **2017**, *46*, 797−815.
(34) Martinez-Ibañez, M.; Sanchez-Diez, E.; Qiao, L.; Meabe, L.; Santiago, A.; Zhu, H.; O'Dell, L. A.; Carrasco, J.; Forsyth, M.; Armand, M.; Zhang, H. Weakly Coordinating Fluorine-Free Polysalt for Single Lithium-Ion Conductive Solid Polymer Electrolytes. *Batter. Supercaps* **2020**, *3*, 738−746.
(35) Li, J.; Zhu, H.; Wang, X.; Armand, M.; MacFarlane, D. R.; Forsyth, M. Synthesis of Sodium Poly[4-styrenesulfonyl-(trifluoromethylsulfonyl)imide]-co-ethylacrylate] Solid Polymer Electrolytes. *Electrochim. Acta* **2015**, *175*, 232−239.
(36) Biesinger, M. C. Accessing the robustness of adventitious carbon for charge referencing (correction) purposes in XPS analysis: Insights from a multi-user facility data review. *Appl. Surf. Sci.* **2022**, *597*, No. 153681.
(37) Dong, X.; Liu, X.; Li, H.; Passerini, S.; Bresser, D. Single-Ion Conducting Polymer Electrolyte for Superior Sodium-Metal Batteries. *Angew. Chem., Int. Ed.* **2023**, *62*, No. e202308699.
(38) Das, S.; Jana, S.; Orsagh, M.; Bys, K.; Mishra, J.; Uchman, M.; Adyam, V. Building Sodium Metal Battery with Polyisoprene-Based Air-Stable Single-Ion Gel Polymer Electrolyte. *ACS Appl. Energy Mater.* **2023**, *6*, 5113−5121.
(39) Meziane, R.; Bonnet, J. P.; Courty, M.; Djellab, K.; Armand, M. Single-ion polymer electrolytes based on a delocalized polyanion for lithium batteries. *Electrochim. Acta* **2011**, *57*, 14−19.
(40) Krajewski, M.; Witowski, A. M.; Liou, S.; Maj, M.; Tokarczyk, M.; Wasik, D. Poly(Vinylidene Fluoride-co-Hexafluoropropylene) Films Filled in Iron Nanoparticles for Infrared Shielding Applications. *Macromol. Rapid Commun.* **2023**, *44* (2023), No. 2300038.
(41) Raju, V. R.; Menezes, E. V.; Marin, G.; Graessley, W. W.; Fetters, L. J. Concentration and molecular weight dependence of viscoelastic properties in linear and star polymers. *Macromolecules* **1981**, *14*, 1668−1676.
(42) De Gennes, P. G. Dynamics of Entangled Polymer Solutions. II. Inclusion of Hydrodynamic Interactions. *Macromolecules* **1976**, *9*, 594−598.
(43) Rubinstein, M.; Helfand, E. Statistics of the entanglement of polymers: Concentration effects. *J. Chem. Phys.* **1985**, *82*, 2477−2483.
(44) Guan, H.; Guo, Z.; Ding, J.; Lian, F. Ionic conductivity and dielectric behavior of novel poly(vinyl formal)-based single-ion-conductor polymer electrolytes. *J. Appl. Polym. Sci.* **2016**, *133*, No. app.43510.
(45) Das, S.; Ghosh, A. Effect of plasticizers on ionic conductivity and dielectric relaxation of PEO-$LiClO_4$ polymer electrolyte. *Electrochim. Acta* **2015**, *171*, 59−65.

(46) Chen, Z.; Kim, G.-T.; Kim, J. K.; Zarrabeitia, M.; Kuenzel, M.; Liang, H.-P.; Geiger, D.; Kaiser, U.; Passerini, S. Highly Stable Quasi-Solid-State Lithium Metal Batteries: Reinforced $Li_{1.3}Al_{0.3}Ti_{1.7}(PO_4)_3$/Li Interface by a Protection Interlayer. *Adv. Energy Mater.* **2021**, *11*, No. 2101339.
(47) Ma, L. A.; Naylor, A. J.; Nyholm, L.; Younesi, R. Sodium-Ion Batteries Strategies for Mitigating Dissolution of Solid Electrolyte Interphases in Sodium-Ion Batteries. *Angew. Chem., Int. Ed.* **2021**, *60*, 4855−4863.
(48) Nigam, A. K.; Suryanarayana, M. V. S.; Gutch, P. K.; Sharma, S. P.; Tomar, L. N. S.; Vijayaraghavan, R. Thermal decomposition studies of riot control agent w-chloroacetophenone (CN) by pyrolysis-gas chromatography−mass spectrometry. *J. Hazard. Mater.* **2010**, *184*, 506−514.
(49) Boaretto, N.; Meabe, L.; Martinez-Ibañez, M.; Armand, M.; Zhang, H. Review—Polymer Electrolytes for Rechargeable Batteries: From Nanocomposite to Nanohybrid. *J. Electrochem. Soc.* **2020**, *167*, No. 070524.
(50) Gebert, F.; Knott, J.; Gorkin, R.; Chou, S.-L.; Dou, S. X. Polymer electrolytes for sodium-ion batteries. *Energy Storage Mater.* **2021**, *36*, 10−30.
(51) Beamson, G. High Resolution XPS of Organic Polymers. *Sci. ESCA 300 Database* **1992**, 188.
(52) Simone, V.; Lecarme, L.; Simonin, L.; Martinet, S. Identification and Quantification of the Main Electrolyte Decomposition By-product in Na-Ion Batteries through FEC: Towards an Improvement of Safety and Lifetime. *J. Electrochem. Soc.* **2017**, *164*, A145−A150.
(53) Muñoz-Márquez, M. A.; Zarrabeitia, M.; Castillo-Martinez, E.; Eguia-Barrio, A.; Rojo, T.; Casas-Cabanas, M. Composition and Evolution of the Solid-Electrolyte Interphase in $Na_2Ti_3O_7$ Electrodes for Na-Ion Batteries: XPS and Auger Parameter Analysis. *ACS Appl. Mater. Interfaces* **2015**, *7*, 7801−7808.
(54) Dias, A. J.; McCarthy, T. J. Dehydrofluorination of poly(vinylidene fluoride) in dimethylformamide solution: Synthesis of an operationally soluble semiconducting polymer. *J. Polym. Sci. Polym. Chem. Ed.* **1985**, *23*, 1057−1061.